Soft Matter

www.rsc.org/softmatter

Volume 9 | Number 46 | 14 December 2013 | Pages 10933–11144

ISSN 1744-683X

RSC Publishing

PAPER

Miguel Piñeirua *et al.*

Capillary buckling of a floating annulus

Soft Matter

RSC Publishing

PAPER

View Article Online
View Journal | View Issue

Capillary buckling of a floating annulus†

Cite this: *Soft Matter*, 2013, **9**, 10985

Miguel Piñeirua,‡*[a] Nana Tanaka,[b] Benoît Roman[a] and José Bico[a]

Received 4th July 2013
Accepted 2nd September 2013

DOI: 10.1039/c3sm51825f

www.rsc.org/softmatter

We describe the out-of-plane buckling of a flexible annulus floating on a bath of water as surfactant molecules are added outside the annulus. The difference in surface tension induces compressive stresses, which result in regular orthoradial wrinkles beyond a critical difference in surface tension. The wrinkles first appear in the vicinity of the inner edge of the annulus and progressively grow as the concentration of surfactant is increased. Conversely, the wavenumber remains constant and relies on a simple balance between gravity and the bending stiffness of the membrane within the range of our experimental parameters. Our experiments fall outside the regimes explored in the literature for similar situations, and we propose an approximate analytical description that completes the existing theoretical grounds.

1 Introduction

Beautiful experiments conducted independently at ESPCI-Paris[1] and UMass Amherst University[2] have shown how the deposition of a tiny droplet at the center of a thin elastic disc floating on a bath of liquid may induce the formation of radial wrinkles around the droplet. The wavenumber was experimentally found to result from the balance between surface tension forces induced by the droplet and the bending stiffness of the membrane while the radial extension of the wrinkles depends on the stretching stiffness. In other words, the wavenumber provides Et^3 (ref. 3) and the length of the wrinkles gives Et, where E and t are the Young's modulus and the thickness of the membrane, respectively.[2] Both quantities may thus be assessed independently. The theoretical description of the problem is nevertheless challenging due to the complexity of the stress distribution in the vicinity of the contact line. A recent theoretical study[3] describes the stress state near the contact line by taking into account the balance between the capillary forces pulling up the contact line and the Laplace pressure pushing down the membrane at the bottom of the droplet. This study assumes a *near threshold* condition where the stress distribution in the flat and wrinkled states is similar. However, the formation of wrinkles is expected to modify the post-buckling stress distribution of a thin membrane in the *far from threshold* regime, which should be relevant to the experiment.[4,5] A very recent study in this regime indeed provides a theoretical prediction for the length of the wrinkles in agreement with experimental data.[6]

Similar experiments have been proposed with the aim of estimating the forces a living cell exerts on a membrane.[7,8] In the experiments by Géminard *et al.*,[7] the center of an elastic disc, preliminary mechanically stretched on a circular frame, is sucked into a small ring, which generates an additional tension. Beyond a critical tension, radial wrinkles appear around the inner ring. The wavenumber is found to be proportional to the radius of the ring while the radial extension of the wrinkles increases with the displacement imposed at the center of the disc. The drop on sheet situation explored by Cerda *et al.*[8] is quite similar although the force is controlled in the experiment instead of the displacement. More recently several studies have been dedicated to the indentation of spherical shells under pressure, which also leads to radial patterns.[9,10] Mechanical information on the stiffness of yeast cells may for instance be inferred from the morphology of the wrinkling pattern.[11] In a different context, orthoradial wrinkles are finally been observed as a projectile impacts a free standing membrane.[12] In this dynamical case, the evolution of the wrinkles is dependent on the propagation of a compression wave through the membrane. Nevertheless, except in the drop on sheet experiment, none of these examples involve surface tension driven buckling.

We propose here a complementary experiment involving a macroscopic annulus floating on water. A difference in surface tension is induced between the inner and outer edges of the annulus by the addition of surfactant molecules with the aim of compressing the annulus. Indeed, soft frames or rings have recently been found to bend or buckle under the surface pressure exerted by surfactant molecules.[13–15] After describing the experimental setup, we shall focus on the case of a narrow annulus where wrinkles extend over the whole width of the annulus. We shall compare this simplified situation with the case of lamellae uniaxially compressed where periodic wrinkles quickly lead to a localized fold.[16,17] We shall finally describe the

[a]*Physique et Mécanique des Milieux Hétérogènes, ESPCI, UPMC, Université Paris Diderot, UMR CNRS 7636, France. E-mail: miguel.pineirua@espci.fr*

[b]*Department of Physics, Ochanomizu University, Bunkyo, Tokyo 112-8610, Japan*

† Electronic supplementary information (ESI) available. See DOI: 10.1039/c3sm51825f

‡ Present address: ENSTA Paristech, Unité de Mécanique, Chemin de la Hunière, 91761 Palaiseau, France.

more general case of wide annuli where wrinkles first appear in the vicinity of the inner edge and extend gradually. In particular, we shall propose a simplified analytical model to describe our experimental observations. We shall also show that our macroscopic experiments explore a different regime from drop on sheet experiments;[1,2] the weight of the underlying fluid sets the wavelength, and the analysis can be developed close to the buckling threshold.

2 Capillary compression

In our experiments we use thin elastic circular annuli cut out from polyvinylsiloxane sheets with an elastic modulus E ranging from 750 to 250 kPa, Poisson ratio $\nu = 0.5$ and thickness t varying from 16 μm to 110 μm. The inner and outer radii of the annuli, a and b respectively, are typically of a few centimeters. The elastic sheets are obtained by spin-coating liquid vinylsiloxane (*Elite double* from *Zhermack*) on a flat surface and letting it cure. Once cut, the annuli are deposited on the surface of a bath of distilled water with an initial surface tension $\gamma = 72$ mN m^{-1}. We generate a difference in surface tension between the interior and the exterior of the floating annulus by adding gently a few droplets of liquid soap outside of the annulus. Two platinum plates, each attached to a force sensor, provide a simultaneous measurement of the surface tension through the classical Wilhelmy plate method[18] inside and outside the disc (Fig. 1). The difference in surface tension is finally tuned by moving a PTFE bar in contact with the water surface. Reduction of the effective surface accessible to the surfactant indeed decreases the outer surface tension γ_o. Since the surfactant is soluble, its diffusion under the annulus and absorption in the inner side would eventually drift down the inner surface tension γ_i. However the duration of an experimental run is short enough to limit this effect (which typically takes tens of minutes).

In addition to standard imaging from above, the out of plane deformation of the disc is monitored through a Free Surface Synthetic Schlieren optical technique developed by F. Moisy.[19] This technique is based on the analysis of the refracted image of a grain pattern visualized through the non-planar interface. An apparent displacement field is deduced from the correlation of two images: a reference image taken while the interface is still undeformed, and a second one taken after deformation. The displacement field is then integrated to reconstruct the instantaneous height field of the surface.

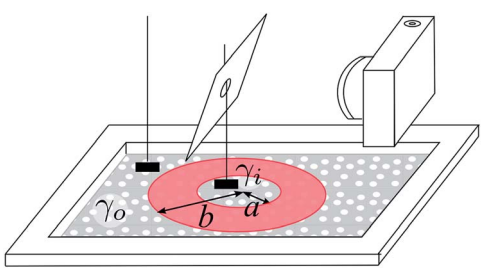

Fig. 1 Experimental setup: an annulus is cut from a thin polymer film and deposited on the surface of water. Surfactant molecules are progressively added outside the annulus and induce a difference in surface tension monitored through standard Wilhelmy plates. Out of plane deformations are deduced from a Free Surface Synthetic Schlieren optical technique.[19]

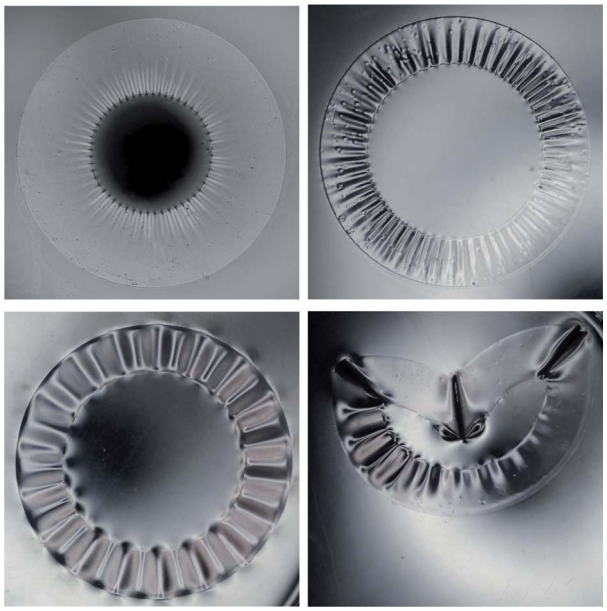

Fig. 2 Typical experiments where wrinkles appear below a critical value of the outer surface tension ($\gamma_1 = 71 \pm 1$ mN m^{-1}): (a) "Wide" annulus, $a/b = 0.35$, $t = 35$ μm, $\gamma_o = 30 \pm 1$ mN m^{-1}, (b) narrow annulus, $a/b = 0.7$, $t = 16$ μm, $\gamma_o = 45 \pm 1$ mN m^{-1}, (c) $a/b = 0.7$, $t = 50$ μm, $\gamma_o = 38.5 \pm 1$ mN m^{-1}, and (d) the same annulus after collapse, $\gamma_o = 32 \pm 1$ mN m^{-1}.

Preliminary experiments conducted with annuli of different geometries are displayed in Fig. 2. Within a time scale shorter than a second, steady radial wrinkles are observed below a critical value of the outer surface tension. Indeed, the stronger tension on the inner boundary tends to reduce the average radius of the annulus, inducing an orthoradial compressive stress. The observed wavenumber remains steady while the concentration of surfactant is increased. Two different situations are observed as a function of the aspect ratio a/b. In the case of wide annuli (small value of a/b), the wrinkles have a finite radial extension at the onset and both extension and amplitude progressively increase as γ_o is lowered. In the case of narrow annuli ($a/b \sim 1$), the initial wrinkles extend along the whole annulus. Eventually, the annulus suddenly collapses below a second value of the outer surface tension (Fig. 2d and a movie supplied in the ESI†).

Addressing first the case of a narrow annulus, we propose that although the annulus is subjected to a tension gradient along the narrow (radial) direction, it exhibits a buckling instability that is nearly identical to the buckling of compressed 1D lamellae.

3 Narrow annulus

We consider first the simpler case of a narrow annulus with a width $w = b - a$ very small in comparison with its average radius $R = (a + b)/2$. Within the limit $w/R \to 0$, such an annulus may be

viewed as the one dimensional band floating on a liquid, and submitted to uniaxial compression.[16,20] We note that the underlying liquid is expected to play a crucial role in the selection of the buckling wavelength. Indeed application of a compressive load on a free band classically leads to a single buckle as higher buckling modes would increase the bending energy. Nevertheless the underlying liquid tends to flatten its surface and favors buckles of higher modes with lower amplitudes. We review the possible buckling patterns due to the "foundation" effect of the underlying liquid (gravity and surface tension), and show that in our experiment, the weight of the displaced liquid is the dominant factor.

3.1 A compressed floating band

We consider a thin elastic band floating on a liquid water compressed under an apparent strain $\varepsilon = |\Delta L|/L$, where L is the total length of the band and ΔL is the imposed displacement (Fig. 3). We start by considering the effect of gravity recently illustrated in a macroscopic experiment.[16]

We compute the wavelength of the wrinkles in terms of scaling arguments based on elastic bending and hydrostatic energies and geometry. Assuming the inextensibility of the thin sheet when wrinkles of wavelength λ and amplitude A appear, length conservation imposes $\varepsilon \sim (A/\lambda)^2$. Since the typical curvature of the band scales as A/λ^2, the global bending energy of the band is given by

$$\mathcal{U}_b \sim B\left(A/\lambda^2\right)^2 Lw, \text{ with } B = \frac{Et^3}{12(1-\nu^2)}, \quad (1)$$

where E and ν are the material's Young's modulus and Poisson ratio, respectively, and t is the thickness of the band. Formation of wrinkles also requires the gravitational energy, which simply scales as:

$$\mathcal{U}_g \sim \rho g A^2 Lw. \quad (2)$$

Minimizing the total energy with respect to λ for an imposed value of ε sets the selected wavelength, the actual pre-factor being obtained through a more precise calculation:[21]

$$\lambda_{eg} = 2\pi(B/\rho g)^{1/4}. \quad (3)$$

Derivation of $\mathcal{U}_m$ to the 2nd order of ε leads to $\mathcal{U}_m = (\rho g B)^{1/2}(2\varepsilon - \varepsilon^2)Lw$. Differentiating the mechanical energy with respect to the displacement $\Delta L = L\varepsilon$ finally gives the corresponding compressive force:

$$f = f_c(1-\varepsilon) \text{ with } f_c = 2(\rho g B)^{1/2} w. \quad (4)$$

Since the load decreases with strain, the wrinkled configuration is mechanically unstable under an applied force. In experiments with a controlled strain,[16] the deformation of the strip is indeed found to localize into a singular fold for $\varepsilon \simeq 0.3$.

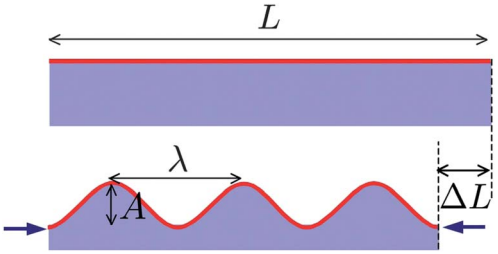

Fig. 3 Wrinkles in a uniaxially compressed sheet floating on a bath of liquid.

3.2 Tension *vs.* gravity, and edge cascade

In addition to the gravitational energy, formation of wrinkles results in an additional capillary energy since menisci are formed along the edges of the wrinkled strip. This additional foundation effect also tends to reduce the amplitude of the wrinkles (and may therefore interfere with the wavelength selection).

The lateral extension of a meniscus is set by the capillary length,[18] $\ell_c = \sqrt{\gamma/\rho g}$, which corresponds to the millimeter length scale for usual liquids. Note that ℓ_c also limits the amplitude of the wrinkles. Indeed inner and outer menisci have to reach the elastic sheet in order to maintain the contact between the sheet and the liquid. Higher amplitudes would lead to delamination.[22] The increase in surface due to the formation of lateral menisci is thus proportional to $(A/\ell_c)^2 L\ell_c$, which leads to the surface energy:

$$\mathcal{U}_s \sim (\gamma\rho g)^{1/2} A^2 L. \quad (5)$$

The previous derivations of the wavelength and buckling threshold are valid within the limit $\mathcal{U}_s \ll \mathcal{U}_g$, *i.e.* $w \gg \ell_c$. As long as the strip is wider than a few millimeters, the buckling wavelength is therefore set by gravity and follows eqn (3). This is the case in experiments involving macroscopic strips.[16]

However, even in the gravity-dominated case, lateral capillary forces may modify the buckling pattern by adding an additional tensile stress to the problem. Indeed recent experiments conducted with ultrathin polystyrene films ($t \sim 100$ nm) floating on water and uniaxially compressed lead not only to the expected buckling wavelength (eqn (3)) in the bulk of the strip, but also to a cascade of wrinkles of wavelengths decreasing from the bulk to the edge.[20] Wrinkles are observed to successively double their frequency in this transition region.[23,24] As described by Vandeparre *et al.*,[24] the scale ℓ_w for such doubling relies on a balance between the bending energy $B(A/\lambda^2)^2 \ell_w L$ and the energy due to tensile forces $\gamma(A^2/\ell_w)L$, which leads to $\ell_w \sim (\lambda^2/t)\sqrt{\gamma/Et} \sim \ell_c$. In the experiments, the width of the transition zone where the bulk wavelength is transformed is indeed observed to be comparable to the capillary length ℓ_c.

Nevertheless, this edge cascade is not observed with thicker materials.[16] Indeed, modifying the wave pattern along the edges also induces stretching strains in the sheet. In terms of scaling, this strain is typically $(A/\ell_w)^2$, resulting in an additional energy cost $Et(A/\ell_w)^4 \ell_w L$. A cascade of wrinkles is thus expected if this additional energy cost is negligible in comparison with the gain in tension energy that drives the formation of a cascade of wrinkles, *i.e.*:

$$A \ll \ell_c \sqrt{\gamma/Et} = \gamma/\sqrt{\rho g E t}. \quad (6)$$

In experiments on ultra thin films,[20] the length scale, $\gamma/\sqrt{\rho g E t} \sim 40$ μm, is about 400 times the thickness of the sheet. This is consistent with the observation of a well defined cascade above the buckling threshold. In contrast, $\gamma/\sqrt{\rho g E t}$ is on the order of 100 μm for our experiments, which is on the order of the thickness of the sheet and below the observed out of plane amplitude of the wrinkles. We thus expect our experiments to lie within the macroscopic regime described by Pocivavsek *et al.* where cascades of wrinkles are not observed along the edges. A comparison of $\gamma/\sqrt{\rho g E t}$ with the thickness of the sheet brings a rule of thumbs for the transition between both regimes; a cascade of wrinkles is indeed expected for $t \ll (\gamma^2/\rho g E)^{1/3}$. Note that a slightly different criterion for the formation of the cascade of wrinkles has been derived by Huang *et al.* based on a softness number that does not depend on the amplitude of the wrinkles.[20]

3.3 Buckling annulus

We assume that a narrow annulus behaves as a 1D band where both ends have been reconnected. The orthoradial force supported by a radial section of the annulus is most easily computed from the integration of the surface pressures along the inner and outer edges of one half of the annulus (see Fig. 4):

$$f_\gamma = \gamma_i a - \gamma_o b. \quad (7)$$

The annulus is expected to wrinkle when this capillary force reaches the threshold buckling force for a one-dimensional band. The critical value of the outer surface tension at the onset of wrinkling is therefore:

$$\gamma_{oc} = \gamma_i a/b - 2(\rho g B)^{1/2}(1 - a/b). \quad (8)$$

This criterion is in good agreement with our experimental observations (Fig. 5). The measured wavelength is also found to follow fairly well the prediction from eqn (3) (Fig. 6, data represented by empty circles).

A linear band uniaxially compressed is expected to collapse immediately if a force slightly larger than the threshold is imposed.[16,17] It might therefore be surprising that, in our experiments, the wrinkling pattern on the annuli remains stable within a certain range of the difference in surface tension. However in our circular geometry, the compression tends to reduce the radius of the annulus, which decreases the compressive force f_γ. If this reduction compensates the negative term in the response of the wrinkled band in eqn (4), the wrinkled annulus should remain stable. More quantitatively, if we apply an apparent compressive strain ε to the mean radius of the annulus, while maintaining a constant width, the inner and outer radii become respectively $a - (a+b)\varepsilon/2$ and $b - (a+b)\varepsilon/2$. A simple derivation of the corresponding force leads to a first order correction in f_γ of $(\gamma_o - \gamma_i)(a+b)\varepsilon/2$. When introduced into the force balance eqn (4), this correction gives the following prediction for the equilibrium strain:

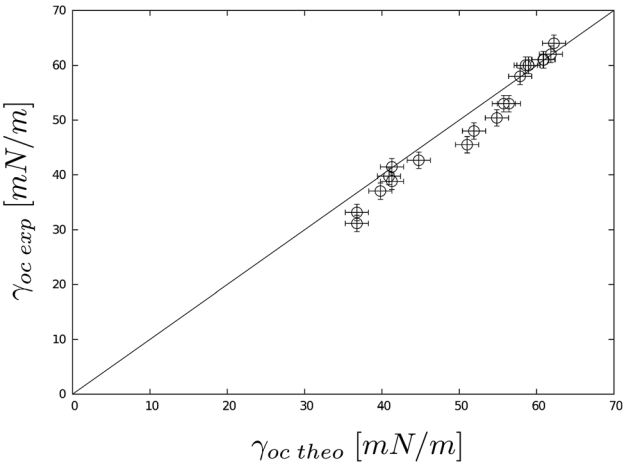

Fig. 5 Comparison of the theoretical estimate of the threshold for wrinkling in the case of narrow annuli (eqn (8)) with the experimental results. Experimental results include annuli of different aspect ratios $0.65 < a/b < 0.9$ and different values of flexural rigidity B.

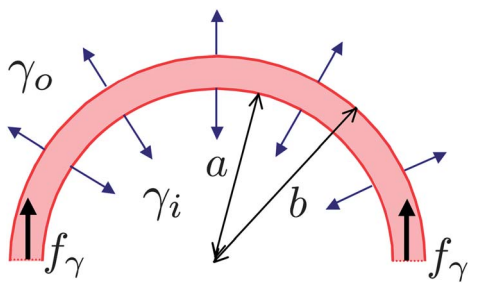

Fig. 4 A difference of outer and inner surface tension γ_o, γ_i results in a compressive force f_γ, as can be seen when isolating force one half of the annulus.

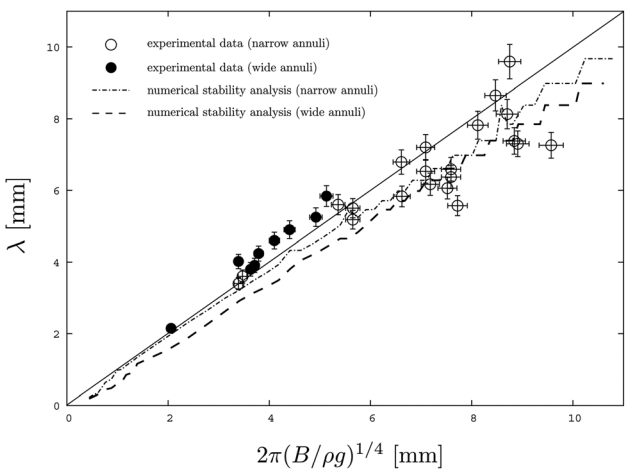

Fig. 6 Wavelength of the wrinkles at the inner edge as a function of the elasto-gravity length scale $2\pi(B/\rho g)^{1/4}$. Circles: experimental data in both narrow (empty dots) and wide (filled dots) annulus regimes. Full line theoretical prediction from eqn (3). Dash-dotted and dashed lines: numerical integration of elastic plane eqn (20) for narrow and wide annuli respectively. The apparent noise observed for large wavelengths results from the integer number of wrinkles.

$$\varepsilon = \frac{2(\gamma_{oc} - \gamma_o)b}{(\gamma_i + \gamma_{oc})(b-a) + (\gamma_{oc} - \gamma_o)(a+b)} \quad (9)$$

To the first order of ε, a decrease in γ_o below the critical value monotonously increases the compressive strain. Determination of a criterion for the collapse of the tube would require a more complex estimation of the energy of the wrinkled annulus and is beyond the scope of this paper.

4 Wide annulus

We now focus on the case of a wider annulus, where the initial wrinkles are observed to remain localized in an area close to the inner edge.

4.1 Stress distribution prior to buckling

While the annulus remains planar, the stress distribution is expected to follow the classical Lamé theory:[25]

$$h\sigma_r = \frac{\gamma_i a^2 - \gamma_o b^2 - \frac{a^2 b^2}{r^2}(\gamma_i - \gamma_o)}{a^2 - b^2}, \quad (10)$$

$$h\sigma_\theta = \frac{\gamma_i a^2 - \gamma_o b^2 + \frac{a^2 b^2}{r^2}(\gamma_i - \gamma_o)}{a^2 - b^2}, \quad (11)$$

where σ_r and σ_θ are the radial and hoop stresses, respectively. Note that $\int_a^b h\sigma_\theta dr$ naturally leads to f_γ defined in eqn (7). Although the radial stress is always positive, the hoop stress can become negative if:

$$\frac{\gamma_o}{\gamma_i} \leq \frac{a^2/b^2 + 1}{2}. \quad (12)$$

In this case the region under orthoradial compression is delimited by $a < r < R^*$, with

$$R^* = a\sqrt{\frac{1 - \gamma_o/\gamma_i}{\gamma_o/\gamma_i - a^2/b^2}}. \quad (13)$$

As in the case of a narrow annulus, such a compression may induce the formation of radial wrinkles on the membranes. Wrinkles are not expected to extend deeply in regions where the membrane is initially under tension ($r > R^*$). Our goal is to understand when out-of-plane buckling occurs and what dictates the wavelength and the extension of the wrinkles. Most of the previous studies focused on the case of an infinite disc (*i.e.* $b/a \to \infty$) in both theoretical[3,4] and experimental[7,8] work. In order to connect our experiment to this limit, we define an effective surface tension at infinity γ_∞ given by

$$\gamma_\infty = \frac{\gamma_o b^2 - \gamma_i a^2}{b^2 - a^2}. \quad (14)$$

This surface tension acting on a virtual disc of infinite diameter would produce the same stresses in the region $a \leq r \leq b$ which is relevant to our finite annulus. The expressions for the stress are then reformulated as:[4]

$$h\sigma_r = \gamma_\infty + (\gamma_i - \gamma_\infty)\frac{a^2}{r^2} \text{ and } h\sigma_\theta = \gamma_\infty - (\gamma_i - \gamma_\infty)\frac{a^2}{r^2}. \quad (15)$$

Introduction of γ_∞ greatly simplifies the condition to obtain a negative hoop stress. Indeed (eqn (12)) becomes:

$$\gamma_i/\gamma_\infty > 2 \quad (16)$$

and the expression for the limit of the region under compression (eqn (13)) is now

$$R^* = a(\gamma_i/\gamma_\infty - 1)^{1/2}.$$

In our experiments γ_i is limited by the surface tension of water (72 mN m^{-1}). The addition of surfactants can only decrease the water surface tension down to a typical value $\gamma_o \sim$ 30 mN m^{-1}, which leads to $\gamma_\infty \sim$ 15 mN m^{-1} for a typical annulus of aspect ratio $a/b = 0.5$. The use of a finite-size annulus ($b < \infty$) thus allows a larger equivalent tension difference to be achieved. The *confinement parameter* defined by Davidovitch *et al.*[4,5] as γ_i/γ_∞ is of order 5. However, the other important parameter introduced in these previous studies, the *bendability*, defined as $a^2\gamma_\infty/B$ is lower than 3000 in our experiments. This parameter is not very large because we are using relatively thick samples (tens of micrometers).

4.2 Buckling conditions

Previous theoretical studies on an ideal case where the hydrostatic pressure is not present suggest that the membrane should buckle if the hoop stress is slightly compressive, the actual threshold being set by a balance between tensile stress and bending stiffness.[4,5] Depending on the confinement and bendability parameters two wrinkling regimes, *near threshold* and *far from threshold*, have been predicted. Different power laws are proposed in both regimes for the number and the length of wrinkles as a function of the bendability parameter. However, the hydrostatic pressure played a major role in setting the buckling threshold and the selected wavelength in our experiments with narrow annuli. We thus propose to analyze our results with wider annuli in the light of these preliminary experiments dominated by gravity. We also keep in mind the relatively low bendability number, and consider that our experiments are close to the buckling threshold.

Considering a compressive stress similar to the critical stress obtained in a narrow band appears as a natural criterion for the threshold, $h\sigma_\theta = -2\sqrt{\rho g B}$, in the vicinity of the inner diameter. In terms of critical surface tension, this condition modifies (eqn (16)) and reads:

$$\left(\frac{\gamma_\infty}{\gamma_i}\right)_{\text{critic}} = \frac{1}{2} - \frac{\ell_{ec}}{\ell_c}, \quad (17)$$

where the *elastocapillary* length[26] and the capillary length are based on the inner surface tension, $\ell_{ec} = \sqrt{B/\gamma_i}$ and $\ell_c = \sqrt{\gamma_i/\rho g}$. We obtain an experimental measurement of the threshold by measuring the amplitude of the wrinkles close to the inner circle as a function of the outer surface tension. The

amplitude increases as the square root of the distance above the threshold, as expected for a supercritical bifurcation, allowing for a precise determination of the threshold (Fig. 7). Our experimental results are in fair agreement with the criterion for the threshold (Fig. 8), without any adjusting parameter. In order to provide a stronger justification for this simple criterion, we perform a numerical linear stability analysis of the Lamé planar solution (eqn (10) and (11)) which provides the buckling threshold, together with the buckling mode (wavelength and radial distribution of the amplitude of the wrinkles at the threshold). This standard analysis is described with more details in appendix 5. The resulting buckling threshold estimated from the numerical integration of eqn (20) is in good agreement with the simplified criterion in eqn (17) (see Fig. 8). We interpret the shift between the experimental data and the predicted values by an additional effect of the meniscus formed along the inner edge.

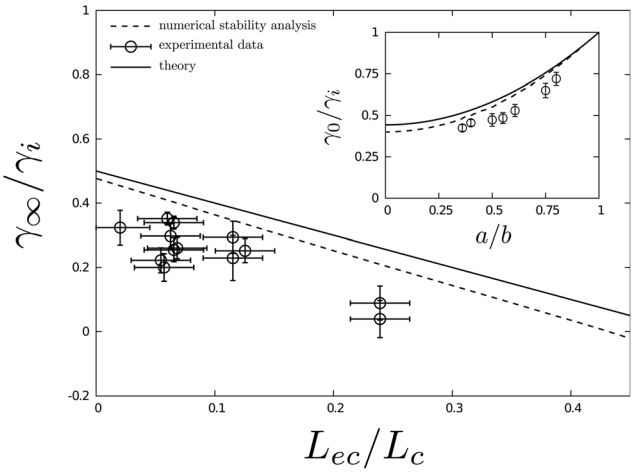

Fig. 8 Evolution of the critical normalized difference in surface tension γ_∞/γ_i as a function of the ratio L_{ec}/L_c: full line, simplified analytical theory (eqn (17)); dashed line, numerical stability analysis of the plate eqn (20); circles, experience. Inset: the relative critical difference as a function of the aspect ratio a/b.

4.3 Wavelength

While the extension length of the wrinkles remains small in comparison with the inner radius of the annulus, it is tempting to compare the wave mode observed in wide annuli with the wavelength selected in a 1D narrow band. We present in Fig. 6 the wavelength of the wrinkles measured along the inner radius. Although the boundary conditions at the end of the wrinkles are different between wide and narrow annuli, the elasto-gravity wavelength $\lambda_{eg} = 2\pi(B/\rho g)^{1/4}$ robustly describes the wrinkles observed in all our experiments (at and above the buckling threshold) (Fig. 6). The numerical stability analysis of the plate equations (appendix 5) confirms this agreement at the threshold (Fig. 6). We conclude that in our system the wavelength is given by a local balance between gravity and bending rigidity.

These experimental and theoretical results are in contrast to theoretical predictions carried out in a different regime dominated by tension. For instance, a balance between bending stiffness and tension dictate the number of wrinkles observed when a drop is deposited on a thin sheet,[2] where gravity does not play any important role.

We note however that a fixed wavelength is obviously not compatible with a constant number of wrinkles. An increase in the difference between γ_i and γ_o tends to increase the extension of the wrinkles. In fact we observe that extended wrinkles tend to split, which limits the deviation of the local wavelength from λ_{eg} (Fig. 9). Although it would be interesting to investigate this wrinkling cascade in a deeper way, the narrow range of the difference in surface tension in our experiment limits such an investigation. The robustness of λ_{eg} may however be probed in a different experiment involving mechanical loads.

4.4 Extension of the wrinkles

We observe experimentally that the extension of the wrinkles increases with the difference in surface tension. The amplitude

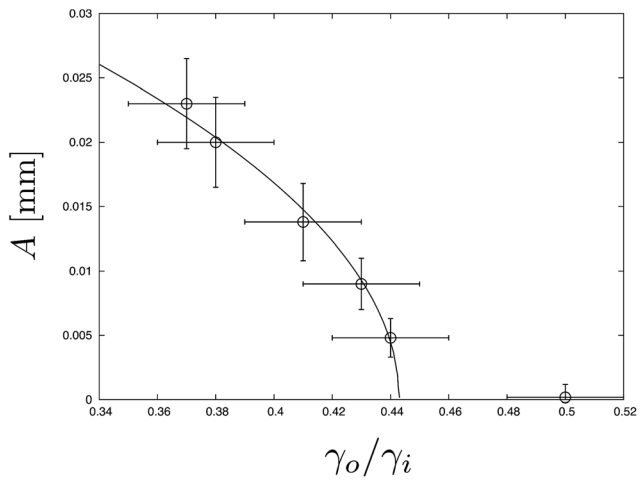

Fig. 7 Evolution of the amplitude as a function of γ_o/γ_i. Symbols: experimental data obtained for a wide annulus $a/b = 0.36$, solid line: fit by the function $A = \alpha\sqrt{(\gamma_o - \gamma_{ocrit})/\gamma_i}$.

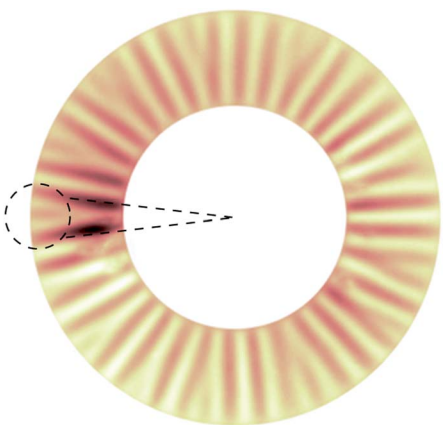

Fig. 9 As the extension of the wrinkles increases new wrinkles appear, which tends to maintain the wavelength in a narrow interval in the vicinity of L_{eg} (see the dotted circle).

of the wrinkles monitored through the synthetic Schlieren technique reaches a maximum close to the inner radius and progressively vanishes away (Fig. 10a). We define the extension length of the wrinkles as the difference between the radius $R_{5\%}$ where the amplitude reaches 5% of the maximal value and the inner radius: $L_w = R_{5\%} - a$. L_w increases progressively as the ratio γ_∞/γ_i is reduced, *i.e.*, as the difference in surface tension is amplified (Fig. 10b). Prediction of the evolution of L_w theoretically is challenging. Indeed, the formation of wrinkles is expected to modify the stress distribution in the annulus. Compressive stresses should eventually become negligible in the *far from threshold* limit. However, we may assume that the stress distribution remains almost preserved in the opposite *near threshold* limit. In the previous section we have defined a simple criterion for buckling based on an extrapolation of the 1D case. Determination of the extent of the wrinkles thus involves more complex plate theory. However, we propose, as a very simplified description, to limit the extent of the wrinkles to regions where the hoop stress is negative ($r < R^*$). Under this condition, the extension of the wrinkles would be given by:

$$L_w = R^* - a = a[(\gamma_i/\gamma_\infty - 1)^{1/2} - 1]. \quad (18)$$

This simple relationship describes relatively well our experimental data. When extrapolated to the buckling threshold eqn (18) also leads to a finite length in incipient wrinkles:

$$L_{wc} = a\left[\left(\frac{1/2 + \ell_{ec}/\ell_c}{1/2 - \ell_{ec}/\ell_c}\right)^{1/2} - 1\right], \quad (19)$$

This length scale would vanish as the membrane becomes very flexible. However the corresponding limit $\ell_{ec} \ll \ell_c$ does not fall within the physical parameters of our experiments. Different behaviors may thus be observed for such a limit.

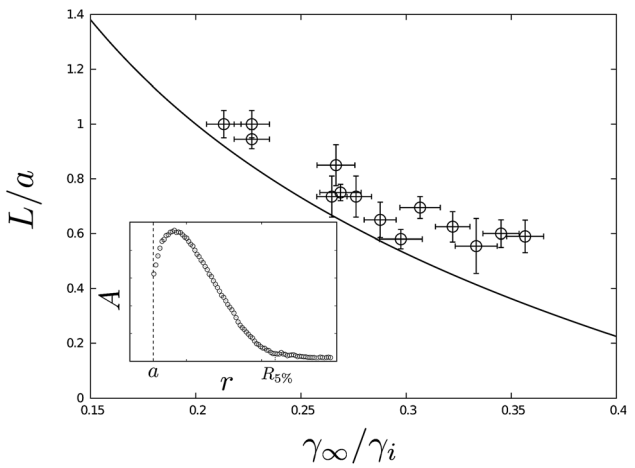

Fig. 10 Evolution of the length of the wrinkles L as a function of the normalized difference in surface tension γ_∞/γ_i. Inset: a typical example of the amplitude of the wrinkles as a function of the radial coordinate.

5 Conclusions

Although the principle of the experiment presented here may appear similar to previous work (such as the case of a drop deposited on a thin sheet), the wrinkling patterns presented here are significantly different. Indeed gravity plays a dominant role in our macroscopic version and leads to a characteristic length scale $\lambda_{eg} \sim (B/\rho g)^{1/4}$. Extended wrinkles are even observed to split in order to maintain this wavelength. Conversely, the wavenumber is fixed in "drop on thin sheet" experiments with the characteristic wavelength around the droplet proportional to $(B/\gamma)^{1/4}a^{1/2}$ (a corresponds to the radius of the drop in this case).[2] In contrast to other experiments involving compressed thin sheets, we do not observe any cascade of wrinkles at the edges of our thick annuli. We indeed expect such a cascade to appear only if the thickness of the sheet in small in comparison with the length scale $(\gamma_i{}^2/\rho g E)^{1/3}$.

Our experiments are also found to correspond to a near threshold situation where the formation of wrinkles does not induce a total collapse of compressive stresses. The threshold is set by a characteristic stress $\sigma_\theta \sim (\rho g B)^{1/2}/t$ and the extension of the wrinkles is reasonably described by the location of $\sigma_\theta = 0$ in Lamé in-plane solution. Conversely, "drop on thin sheet" experiments are far from the threshold and the extension of the wrinkles was found to be empirically set by $a(Et/\gamma)^{1/2}$, while a recent analysis predicts dependence on $a(Et/\gamma)^{1/3}$ instead.[6]

As a conclusion we have found a different regime of radial wrinkling induced by surface tension forces; in contrast to experiments at the scale of the capillary length $(\gamma/\rho g)^{1/2}$, gravity dominates here and imposes a given wavelength. We have however only explored this regime close to the buckling threshold. The use of ultra thin film samples at the centimeter scale would allow characterization of the "far from threshold" limit of this gravity regime, which remains completely unexplored. We believe that this radial wrinkling regime with an imposed wavelength would exhibit a behavior as rich and stimulating as the tension-driven regime which has attracted strong attention lately, with distinct features such as an extended wrinkling cascade.

Appendix

Linear stability analysis of buckling

We describe here the standard stability analysis of the stretched annulus presented in more detail by Davidovitch *et al.*[5] We consider the linear elastic plate equation:[27]

$$B\nabla^4 w - \sigma_r t\frac{\partial^2 w}{\partial r^2} - \sigma_\theta t\left(\frac{1}{r}\frac{\partial w}{\partial r} + \frac{1}{r^2}\frac{\partial^2 w}{\partial \theta^2}\right) + \rho g w = 0, \quad (20)$$

where w is the vertical deflection of the sheet, and we impose σ_r, and σ_θ as the Lamé's stress solution (eqn (10) and (11)). In this equation, the first term represents the bending rigidity, the two central terms are due to in-plane stresses, whereas the last term represents the hydrostatic pressure.

We look for a non-zero solution of eqn (20) in the form $w = f(r)\sin(m\theta)$. The plate is free of forces or torques along the inner and outer radii, and one would impose three boundary conditions: zero axial torque M_r,

$$\frac{M_r}{B} = \left[\frac{\partial^2 w}{\partial r^2} + \nu\left(\frac{1}{r}\frac{\partial w}{\partial r} + \frac{1}{r^2}\frac{\partial^2 w}{\partial \theta^2}\right)\right] = 0 \text{ for } r = a, b \qquad (21)$$

zero transverse torque $M_{r\theta} = B(1-\nu)\frac{\partial}{\partial r}\left(\frac{1}{r}\frac{\partial w}{\partial \theta}\right)$ and zero vertical force $Q_r = B\frac{\partial}{\partial r}\Delta w$. However, only two conditions on each boundary ($r = a$, b) are needed for the fourth order eqn (20). In fact, the conditions on Q_r and $M_{r\theta}$ are coupled into a single condition due to the infinite shear rigidity assumed within classical plate theory[27] which reads

$$Q_r - \frac{1}{r}\frac{\partial M_{r\theta}}{\partial \theta} + h\sigma_r\frac{\partial w}{\partial r} = 0 \text{ for } r = a, b \qquad (22)$$

The form $w = f(r)\sin(m\theta)$ leads to a linear 4th order ordinary differential equation on $f(r)$, with four boundary conditions. In general this linear system has one solution, $f = 0$, but for a critical value of the outer surface tension γ_∞ (the buckling threshold) a non-zero solution exists. This boundary value problem can be solved numerically for any value of the wavenumber m. We then find the wavenumber m which corresponds to the lowest value of the buckling threshold.

This procedure gives numerical computation of the buckling threshold and the buckling mode (wavelength and radial distribution of the amplitude at the threshold) which can be compared with experiments.

Acknowledgements

We thank very much N. Menon for participating in the preliminary version of this experiment, B. Davidovitch for intense discussions and careful reading of the manuscript and B.Audoly and E.Cerda for help with stability analysis. N. Tanaka was supported by the International Training Program from the Japan Society for the Promotion of Science. This work was also partly supported by μMAST-Belspo.

References

1 H. Bodiguel, Ph.D. thesis, Universit Pierre & Marie Curie, Paris 6, 2006.
2 J. Huang, M. Juszkiewicz, W. de Jeu, E. Cerda, T. Emrick, N. Menon and T. Russell, *Science*, 2007, **317**, 650–653.
3 D. Vella, M. Adda-Bedia and E. Cerda, *Soft Matter*, 2010, **6**, 5778–5782.
4 B. Davidovitch, R. Schroll, D. Vella, M. Adda-Bedia and E. Cerda, *Proc. Natl. Acad. Sci. U. S. A.*, 2011, **108**, 18227–18232.
5 B. Davidovitch, R. Schroll and E. Cerda, *Phys. Rev. E: Stat., Nonlinear, Soft Matter Phys.*, 2012, **85**, 066115.
6 R. Schroll, M. Adda-Bedia, E. Cerda, J. Huang, N. Menon, T. Russel, K. Toga, D. Vella and B. Davidovitch, *Phys. Rev. Lett.*, 2013, **111**, 014301.
7 J. Géminard, R. Bernal and F. Melo, *Eur. Phys. J. E*, 2004, **15**, 117–126.
8 E. Cerda, *J. Biomech. Eng.*, 2005, **38**, 1598–1603.
9 D. Vella, A. Ajdari, A. Vaziri and A. Boudaoud, *Phys. Rev. Lett.*, 2011, **107**, 174301.
10 R. Bernal, C. Tassius, F. Melo and J.-C. Géminard, *Eur. Phys. J. E*, 2011, **34**, 13.
11 D. Vella, A. Ajdari, A. Vaziri and A. Boudaoud, *J. R. Soc., Interface*, 2012, **9**, 448.
12 R. Vermorel, N. Vandenberghe and E. Villermaux, *Proc. R. Soc. A*, 2009, **465**, 823–842.
13 Y. Hu, K. Lee and J. Israelachvili, *Langmuir*, 2003, **19**, 100–104.
14 Z. Zell, S. Choi, L. Leal and T. Squires, *Appl. Phys. Lett.*, 2010, **97**, 133505.
15 N. Adami, A. Delbos, B. Roman, J. Bico and H. Caps, *J. Fluids Struct.*, 2013, submitted.
16 L. Pocivavsek, R. Dellsy, A. Kern, S. Johnson, B. Lin, K. Y. C. Lee and E. Cerda, *Science*, 2008, **320**, 912–916.
17 H. Diamant and T. Witten, *Phys. Rev. Lett.*, 2011, **107**, 164302.
18 P. de Gennes, F. Brochard-Wyard and D. Quéré, *Capillarity and Wetting Phenomena: Drops, Bubbles, Pearls, Waves*, Springer-Verlag, New York, 1st edn, 2003.
19 F. Moisy, M. Rabaud and K. Salsac, *Exp. Fluids*, 2009, **46**, 1021–1036.
20 J. Huang, B. Davidovitch, C. Santangelo, T. Russel and N. Menon, *Phys. Rev. Lett.*, 2010, **105**, 038302.
21 S. Milner, J.-F. Joanny and P. Pincus, *Europhys. Lett.*, 1989, **9**, 495–500.
22 T. Wagner and D. Vella, *Phys. Rev. Lett.*, 2011, **107**, 044301.
23 B. Davidovitch, *Phys. Rev. E: Stat., Nonlinear, Soft Matter Phys.*, 2009, **80**, 025202.
24 H. Vandeparre, M. Piñeirua, F. Brau, B. Roman, J. Bico, C. Gay, W. Bao, C. Lau, P. Reis and P. Damman, *Phys. Rev. Lett.*, 2011, **106**, 224301.
25 S. Timoshenko and S. Woinowsky-Krieger, *Theory of Plates and Shells*, McGraw-Hill, Singapore, 2nd edn, 1959.
26 B. Roman and J. Bico, *J. Phys.: Condens. Matter*, 2010, **22**, 493101.
27 E. Mansfield, *The Bending and Stretching of Plates*, Cambridge University Press, 1989.

